p53 Promotes Ferroptosis in Macrophages Treated with Fe_3O_4 Nanoparticles

Cong Wu[1,2], Boyou Zhang[1,2], Zhiming Shen[1,2], Fei Sun[1,2], Yi Lu[1,2], Lei Yuan[1,2], Guozhong Zhang[1,2], Zhihao Wang[1,2], Hongcan Shi[1,2*]

[1] Clinical Medical College, Yangzhou University, Yangzhou, China； [2] Institute of Translational Medicine, Medical College, Yangzhou University, Yangzhou, China；

First auther: Cong Wu; wucong987@163.com

Corresponding author: Hongcan Shi； Email: shihongcan@yzu.edu.cn

Abstract

Background: Fe_3O_4 nanoparticles (NPs, also known as iron oxide NPs; IONPs) have high biocompatibility and low biotoxicity. They are widely used in the field of biotechnology for targeted delivery, image formation, and photothermal therapy. NP biodistribution is determined by macrophage capture in vivo, and recently, the induction of macrophage polarization into the M1 phenotype by IONPs has become a hot topic in research. Previous research has shown that IONPs can induce ferroptosis of ovarian cancer cells and ischemic cardiomyocytes. In this study, we exposed macrophages to synthesized Fe_3O_4 NPs (100 nm in diameter) and determined the effects of NPs in inducing cell death by RNA sequencing.

Results: We observed that after 48 h exposure to NPs, there was a change in the macrophage phenotype and a reduction in cell viability. Then, we demonstrated that NPs could induce macrophage cell damage by increasing intracellular reactive oxygen species and by repressing the mitochondrial membrane potential. Furthermore, we investigated the underlying mechanisms of ferroptosis of macrophages using RNA sequencing and change in ultrastructural morphology, and found that ferroptosis was caused by the upregulation of p53 expression and inhibition of SLC7A11 expression, as their protein levels after 48 h exposure to Fe_3O_4 NPs were consistent with erastin-induced ferroptosis.

Conclusions: These results provide an insight into the molecular mechanisms underlying ferroptosis induced by Fe_3O_4 NPs in macrophages and provide a basis for the biotoxicity study of Fe_3O_4 NPs in vivo**.**

Keywords: Fe_3O_4 nanoparticle, macrophage, polarization, ferroptosis, p53

Background

Fe_3O_4 NPs are among the most widely used magnetic nanoparticles in the field of biomedicine owing to their outstanding magnetism, low toxicity, biocompatibility, biodegradability, and easy aggregation and oxidation. In the medical field, they have used in a variety of applications, such as (i) targeted delivery of drug or gene [1-3]; (ii) improving the quality of the contrast in magnetic resonance imaging (MRI) and photothermal therapy [4, 5]; (iii) detection, diagnosis, and radiation treatment of cancerous cells [6, 7]. Zanganeh et al. discovered that ferumoxytol inhibits cancer growth via the polarization of tumor-associated macrophages (TAMs) into M1 phenotypes [8]. The repolarization of TAMs into antitumorigenic macrophages is a potential target for cancer therapy [9-11]; therefore, Fe_3O_4 NPs have been a major focus of recent research. The NP biodistribution in vivo is determined by

the capture of macrophage and subsequent degradation by macrophages [12]. However, except phenotypic changes, the effects of Fe_3O_4 NPs on macrophages remain poorly understood.

Ferroptosis is an oxidative type of regulated cell death caused by a metabolic disorder of intracellular lipid oxides and morphologically distinct from other forms of cell death. It was first formally described as an iron-dependent form of erastin-induced non-apoptotic cell death [13]. Ferroptosis is characterized by abnormal levels of iron ions and excessive reactive oxygen species (ROS) generation. When the antioxidant capacity of cells is weakened, ROS accumulates, leading to an imbalance in intracellular redox and the induction of ferroptosis. In addition to morphological changes, such as the rupture of the outer mitochondrial membrane, small mitochondria with a condensed membrane, and loss or decrease in mitochondrial cristae are also mediated by ferroptosis [14]. Ferroptosis induction is associated with multiple diseases and has recently gained substantial attention as a target for cancer treatment [14]. It is reported that iron oxide NPs induced ferroptosis in few cancer cells [17, 18] and ischemic cardiomyocytes [19].

With respect to our current understanding of the mechanism underlying ferroptosis, glutathione peroxidase 4 (GPX4) reduces cytotoxicity by converting glutathione (GSH) to oxidized glutathione (GSSH), and the inhibition of GPX4 causes accumulation of lipid peroxides induces ferroptosis. The glutathione peroxidase pathway can directly inhibit GPX4, which is further regulated by system Xc-, an amino acid anti-transporter composed of heterodimeric disulfide bound to xCT (*SLC7A11*). GSH biosynthesis, cysteine availability, and the proper functioning of GPX4 are crucial for regulating ferroptosis [20, 21]. Jiang et al. found that p53 promotes ferroptosis in fibroblasts, the human breast cancer cell line MCF7, and the human osteosarcoma cell line U2OS via trans-repression of solute carrier family 7 member 11 (*SLC7A11*) expression. This provided the first evidence for the induction

of p53 in response to ferroptosis [22, 23]. At present, the regulatory effects of p53 in ferroptosis have only been detected in cancer cells [24, 25].

Herein, we evaluated the effects of Fe_3O_4 NP treatment on macrophage phenotype. We observed that treatment with Fe_3O_4 NPs caused macrophages to polarize into the M1 phenotype, accompanied with a reduction in cell viability. Using RNA-seq, we found that NPs induced ferroptosis in macrophages via upregulation of *p53* expression and downregulation of *SLC7A11* expression. We used erastin-treated Ana-1 cells as positive control, and the ferroptosis of macrophages was verified by observing the changes in the ultrastructure of the mitochondria and by assessing the expression levels of TFR, p53, and xCT. Moreover, we demonstrated p53 regulation of ferroptosis in macrophages; this is the first evidence of p53 mediated ferroptosis in cells other than cancer cells.

Results

Characterization of Fe_3O_4 NPs and effects on cell viability

Ultramicrographs (TEM, Fig. 1a; SEM, Fig. 1b) show that the NPs were spherical and uniform in shape. The hydrodynamic diameters of NPs were measured by dynamic light scattering (DLS; Nano ZS90, Malvern, England), and the average hydrodynamic diameters of NPs (Fig. 1c) were 104 ± 3.25 nm, in good agreement with the TEM results. The zeta potentials (Fig. 1d) were -28.03 ± 1.3 mV. These results indicated that the NPs had excellent properties and stability in ultrapure water

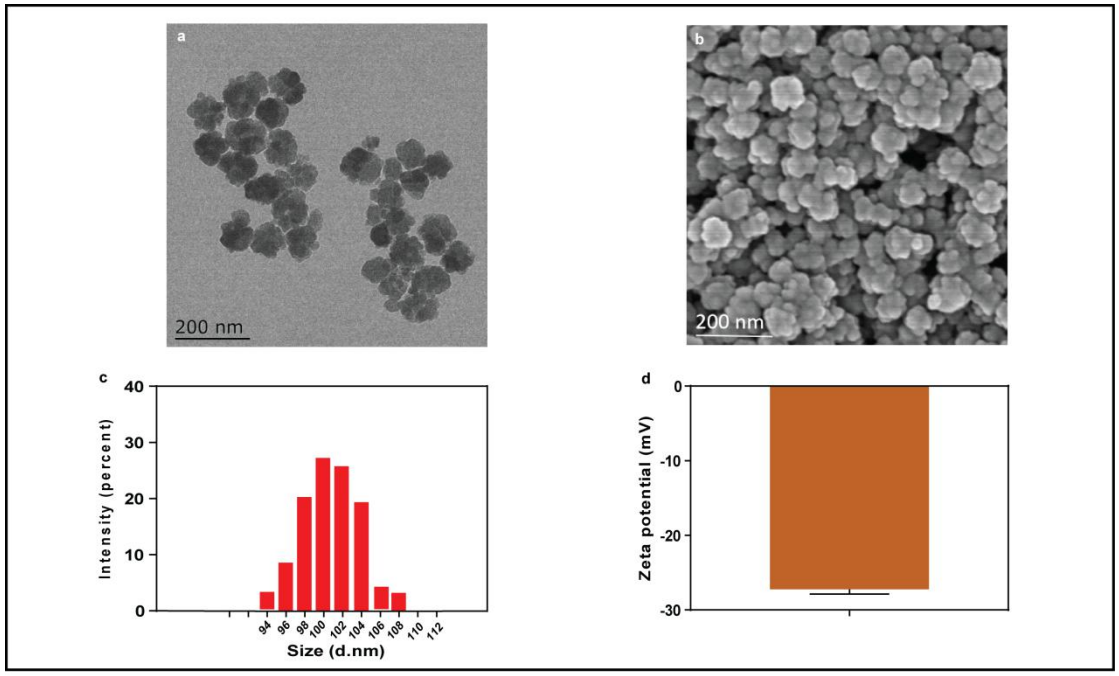

Figure 1. Characterization of Fe_3O_4 NPs. (a) Transmission electron micrograph, Ob: 50000×; (b) Scanning electron micrograph, Ob: 50000×; (c) ζ-potential of NPs in Milli-Q water; (d) determination of NPs size by DLS.

Ana-1 cells were exposed to various concentrations of NPs for 24 and 48 h, and cell viability was determined. As seen in Fig. 2a, NP treatment inhibited the proliferation of Ana-1 cells in a dose- and time-dependent manner. When the concentration was less than 400 μg/mL, there was no significant decrease in cell viability after treatment for 24 h. However, there was an approximately 8–10% reduction in the viability of cells. In figure 2b, when the exposure time was extended to 48 h, the cell viability decreased significantly (by approximately 25%) ($p < 0.05$). Therefore, in subsequent analyses, 400 μg/mL NPs was used. Cell viability was significantly inhibited at higher concentrations (500 μg/mL) ($p < 0.01$).

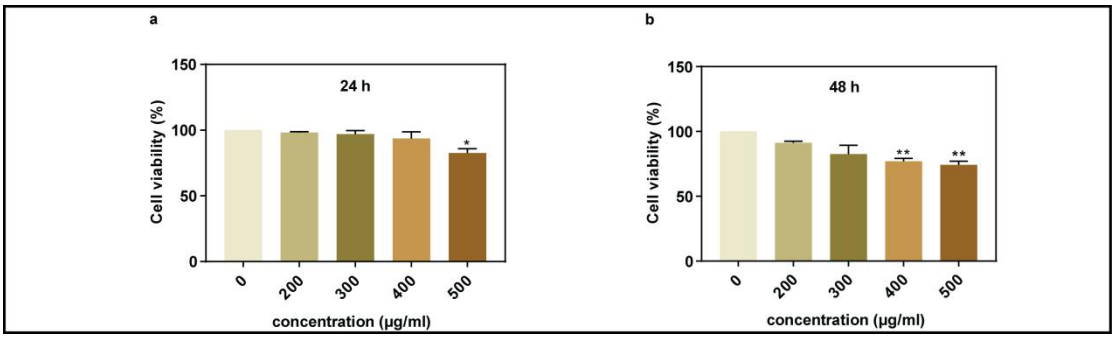

Figure 2. Effects of gradient concentrations of nanoparticles (NPs) on cell viability after (a) 24 h and (b) 48 h. Control cells cultured in nanoparticle-free medium were processed in parallel with the treatment groups. Results of the CCK-8 assay are expressed as percentage relative to the control. Data are expressed as means ± SEM, *$p < 0.05$; **$p < 0.01$ vs Control.

Effect of Fe_3O_4 NPs on macrophage phenotypes

TAMs can be functionally categorized into M2 macrophages [27]. M1 macrophages are characterized by a high expression of inducible nitric oxide synthase (iNOS), high levels of arginase-1 (Arg-1) and anti-inflammatory (IL-10) are the markers of M2 macrophages. Ana-1 cell line is an inactivated bone marrow monocyte-derived macrophage line and is classified as macrophages; however, its protein expression pattern is similar to that of the M1 phenotype .

Cells were incubated with gradient concentrations of NPs for 24 h and 48 h, while untreated cells were used as control. As shown in Fig. 3a, Arg-1 expression was extremely low in cells treated with NPs at concentrations of ≥200 μg/mL ($p < 0.001$). The expression levels of iNOS in cells treated with NPs at ≥300 μg/mL were 1.5- to 3-fold higher than those in the control ($p < 0.05$; $p < 0.01$). As shown in Fig. 3b, an RT–qPCR analysis revealed that the mRNA levels of *iNOS* at ≥400 μg/mL were significantly higher than those in the untreated cells ($p < 0.05$; $p < 0.01$). *ARG-1* mRNA levels were significantly lower in all experimental groups than in the control group ($p < 0.001$), consistent with the

results obtained by western blotting. The levels of *IL-10* in all groups decreased markedly ($p < 0.001$), and low *IL-10* expression is a characteristic feature of M1 macrophages. These results suggest that NPs at ≥300 μg/mL could polarize Ana-1 macrophages to the M1 phenotype, consistent with previous results [8, 30]. Notably, the protein levels of macrophages treated with NPs for 24 h (Fig S1a) did not change significantly ($p>0.05$), suggesting that the macrophage phenotype did not change.

After the construction of the TAM models, they were incubated with or without NPs for another 24 h or 48 h. After incubating for 24 h (Fig S1b), the protein levels did not change significantly. The proteins in the 48 h group were examined by western blotting (Fig. 3c). Compared to levels in the control group, which were untreated cells, TAMs showed a significant increase (2- to 2.5-fold) in the expression of Arg-1 ($p < 0.05$). The levels of iNOS were lower in TAMs than in the control group, but the difference was not statistically significant, indicating that the TAM model contained a mixture of M1/M2 phenotypes [31]. iNOS expression levels in NP-treated TAMs were 4- to 5-fold higher than those in TAMs ($p < 0.01$), and Arg-1 expression levels were 5-to 7-fold lower ($p < 0.01$). We also examined the mRNA levels of *iNOS, Arg-1*, and *IL-10* (Fig. 3d). Significant reductions in the mRNA levels of *Arg-1/iNOS* (1.5- to 2-fold) and *IL-10/iNOS* levels (55- to 57-fold) were observed in the NP-treated TAMs compared with the control group ($p < 0.01$). These genes and protein expression analyses confirmed the polarizing effect of NPs on TAMs.

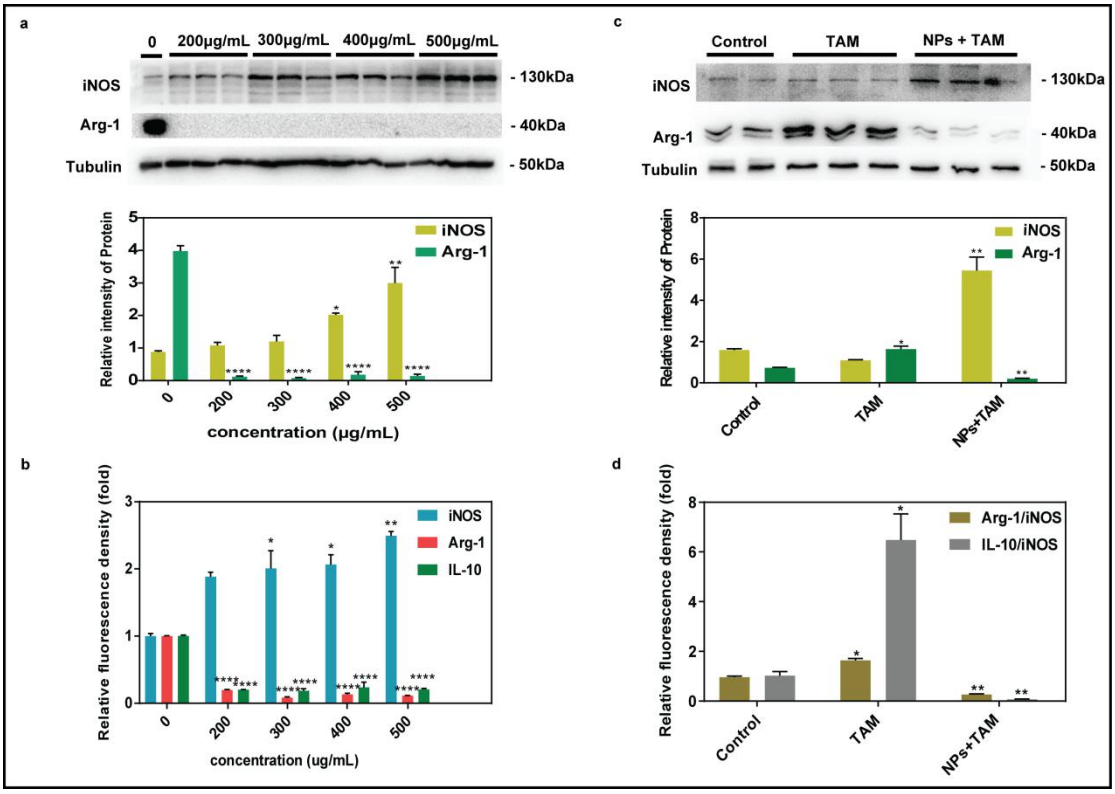

Figure 3. Effect of NPs on the change of macrophages phenotype. (a) Protein levels of iNOS and Arg-1 in Ana-1 cells incubated with 200, 300, 400, and 500 μg/mL NPs examined by western blotting; (b) mRNA levels of *iNOS, Arg-1*, and *IL-10* in Ana-1 cells treated with various concentrations of NPs; (c) Expression levels of iNOS and Arg-1 in the tumor-associated macrophage (TAM) model incubated with or without NPs; (d) The ratios of *Arg-1/iNOS* and *IL-10/iNOS* assayed by reverse transcription–quantitative PCR. Protein levels are shown relative to untreated Ana–1 cells as control. The quantification of protein levels was achieved by calculating the signal intensity ratio of iNOS and Arg-1 to the internal control (Tubulin); The mRNA levels were normalized to those of *GAPDH*. Data from at least three independent experiments were used for quantification. Data are expressed as means ± SEM, and *$p < 0.05$; **$p < 0.01$; ****$p < 0.001$.

Uptake of intracellular iron

Ana-1 cells were incubated with NPs for 4, 8, 12, and 24 h at 37°C, and intracellular iron contents were measured by ICP-ACE (Fig. 4a). In all samples, the uptake of nanoparticles increased significantly in 8 h (140.29 pg/cell). The rate of uptake gradually slowed and reached a plateau at 12 h (134.74 pg/cell). This might reflect the depletion of free NPs in the culture medium. At 24 h, the decrease in the intracellular content may be due to exocytosis. The cellular NP content in the macrophages was visualized by Prussian blue staining (Fig. 4b), and the expected Prussian blue reaction was seen. We observed intracellular red fluorescence from lysosomes; the extensive colocalization of red fluorescence from the probes and NPs can be observed in Fig. 4c and d. These results indicated that NPs accumulated in lysosomes after internalization.

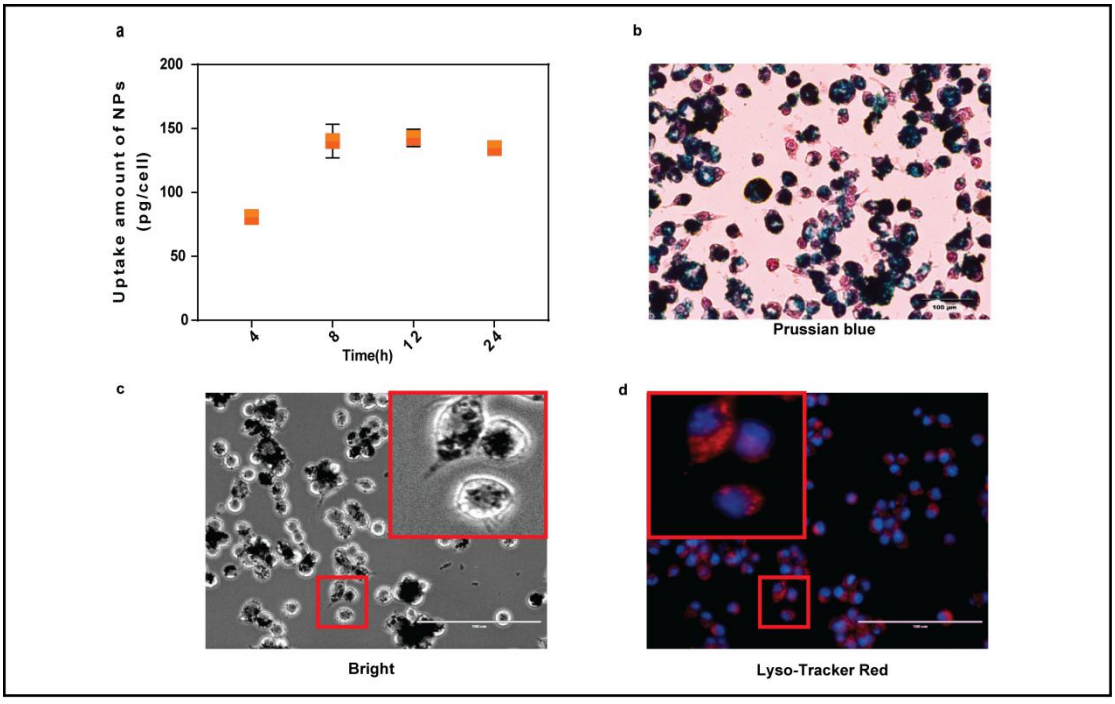

Figure 4. Quantification of intracellular localization of NPs. (a) Cellular iron contents measured by ICP-ACE; (b) Presence of iron in cells are visualized by Prussian blue staining; (c, d) Colocalization of intracellular NPs with lysosomes revealed by staining with Lyso-Tracker Red fluorescence probes; Ob: 200×.

Mitochondrial damage triggered by Fe_3O_4 NPs

After NPs are degraded into iron ions in lysosomes, iron ions induce oxidative stress by generating ROS [31]. Ferroptosis is a type of ROS-dependent regulated cell death [31], mitochondrial damage is the most common feature of this process which caused by intracellular ROS [18]. As determined by flow cytometry (FCM) (Fig. 5a, b), the intracellular ROS content at 24 h was nearly 20–22% higher than that in the control group, with no significant difference. At 48 h, the contents were about 12% higher than those at 24 h, and 32-40% higher ($p < 0.05$). This means as the exposure time increased, intracellular ROS also increased. As shown in Fig. 5c, we compared MMP changes by the green/red fluorescence ratio. The 24 h group showed slight mitochondrial damage and relatively few inactivated cells, the ratio in the 48 h group was significantly higher than that in the control group ($p < 0.005$). As seen in Fig. 5, red fluorescence was lower in the 48 h group (g) than in the control (d) and 24 h group (f), while green fluorescence was similar to that of the CCCP group (e), consistent with mitochondrial damage. The results shown that as the exposure time increased to 48 h, more mitochondria were destroyed. Accordingly, the increase in intracellular ROS was accompanied by the repression of MMP in the 24 h and 48 h groups, indicating that mitochondrial damage depended on ROS levels in cells.

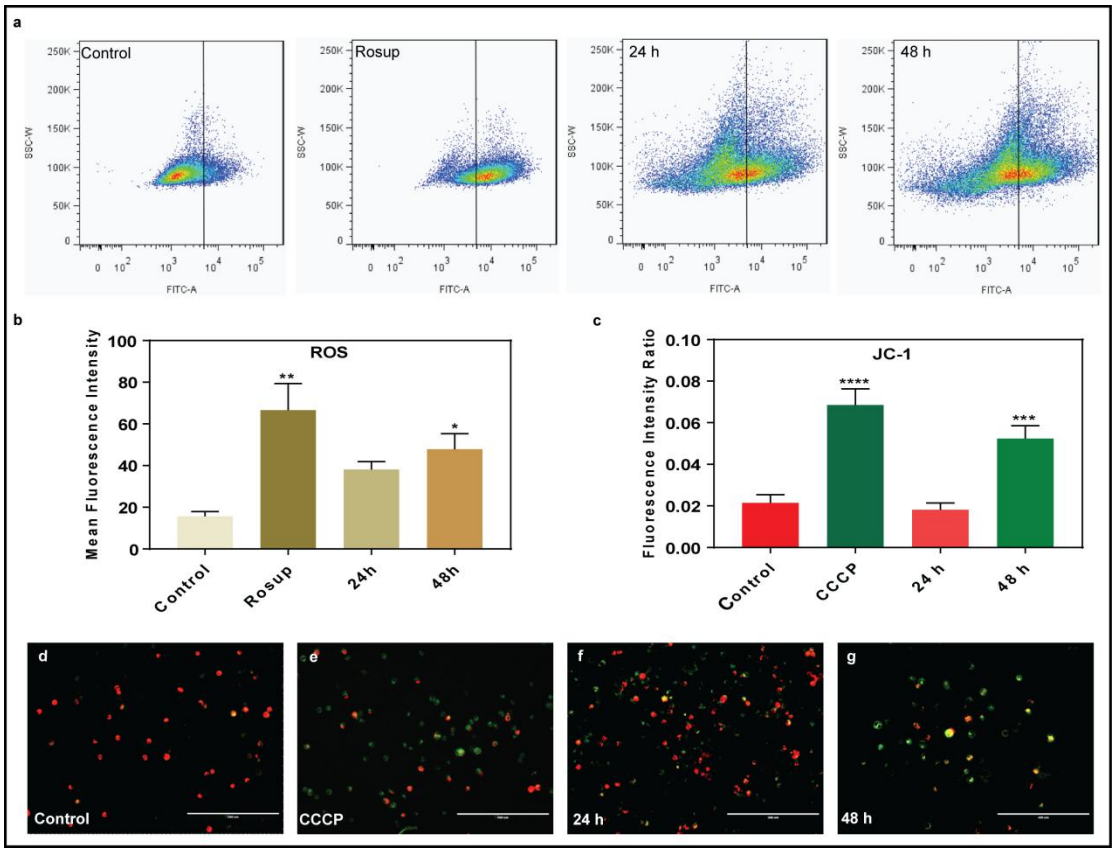

Figure 5. Determination of intracellular ROS and MMP levels. (a, b) Trends in ROS generation detected by FCM. When the MMP is high, the JC-1 probe is dispersed in a multimeric form in the mitochondrial matrix (red fluorescence; Ex = 585 nm, Em = 590 nm). JC-1 is dispersed in the mitochondrial matrix in a free state when the MMP is low (green fluorescence; Ex = 514 nm, Em = 529 nm); (c) Graphical representation of the green/red fluorescence intensity ratios; (d) Untreated cells used as negative control; (e) CCCP treatment for 20 min used as positive control; JC-1 stained micrographs at 24 h (f) and 48 h (g); Ob: 200×; *$p < 0.05$; **$p < 0.01$; ***$p < 0.005$; ****$p < 0.001$ vs Control.

Ferroptosis of macrophages induced by Fe_3O_4 NPs

To further explore the influence of NPs on macrophages, the expression levels of all genes were evaluated by RNA-seq (Fig. 6a). We found that NPs induce ferroptosis by upregulating *p53* and downregulating *SLC7A11*, a key component of the cystine/glutamate transporter. Transferrin

receptor (TFR) mediates the entry of iron-containing ferritin into cells, and Feng et al. [34] have shown that TFR accumulation is a hallmark of ferroptosis. According to the RNA-seq results, NPs increased the level of TFR, consistent with the expression characteristics of ferroptosis.

A previous study has reported that the activation of *p53* can induce ferroptosis by inhibiting system Xc^- activity. Erastin is a typical ferroptosis-inducer, an oncogenic RAS-selective lethal small molecule [35]. Recent findings suggest that erastin can also activate p53 and enhance ferroptosis [36, 37]. Therefore, we used erastin (25 μM)-treated Ana-1 cells for 24 h as a positive control for ferroptosis [38]. We determined the protein levels of TFR, p53, and xCT (*SLC7A11*) by western blotting to verify the sequencing results and further evaluate the ferroptosis pathway. As shown in Fig. 6b, TFR levels were approximately 1-fold higher in the erastin group than in the control group ($p < 0.001$), indicating that the expression of TFR is an indicator of ferroptosis. The expression levels of TFR at 24 h and 48 h were significantly higher than those in the control group by approximately 0.75- and 1.1-fold, respectively ($p < 0.001$). The protein levels of p53 in both the NP-treated group and erastin group were higher than those in the control group by approximately 1- and 2-fold ($p < 0.001$). The expression levels of xCT in all treatment groups were significantly lower than those in the control group ($p < 0.005$; $p < 0.001$), consistent with the RNA-seq results and with previous results for erastin-induced ferroptosis [38].

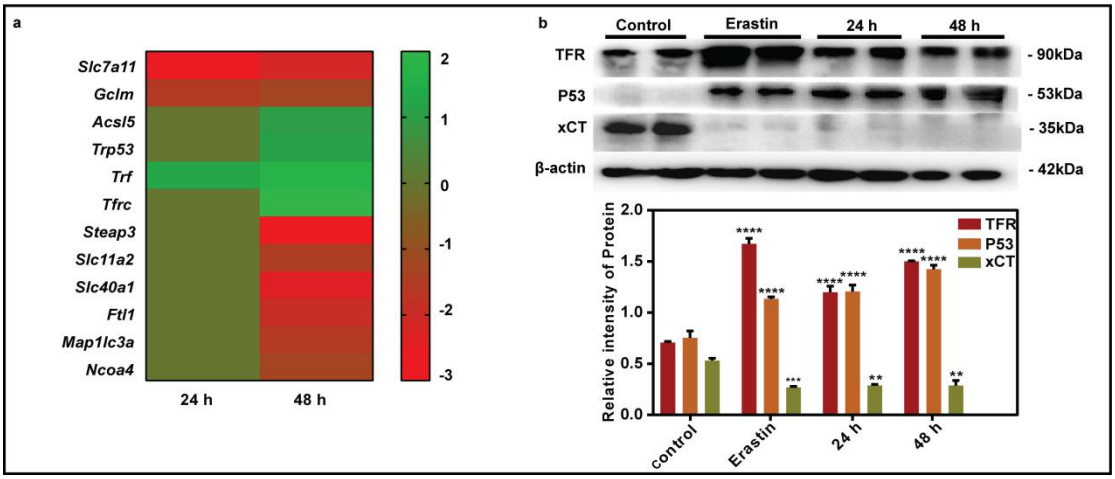

Figure 6. RNA-seq, ultrastructural change of mitochondria, and verification of protein expression associated with ferroptosis. (a) Heat map visualization of the expression of various key genes of the ferroptosis pathway; (b) Protein levels of TFR, p53, and xCT (SLC7A11) in the 24 h, 48 h, and erastin groups. Untreated Ana-1 cells used as control; quantification of protein levels was achieved by calculating the signal intensity ratio of target protein bands to the internal control bands (β-actin). Data are expressed as means ± SEM, and **$p < 0.01$; ***$p < 0.005$, ****$p < 0.001$ vs Control.

Ultrastructure of mitochondria in macrophage

Ultrastructural changes in the mitochondria, such as a volume reduction, outer mitochondrial membrane disruption, and disappearance of the mitochondrial cristae [40, 41] are considered as hallmarks of ferroptosis [42]. As shown in Fig. 7b, shrunken mitochondria and fractured mitochondrial cristae are seen in the erastin-treated cells. Ferroptosis can be characterized at a morphological level by the presence of shrunken mitochondria [22]. in addition to the normal mitochondria, ruptured mitochondrial cristae are also observed in the 24 h group (Fig. 7c). At 48 h (Fig. 7d), we observed

mitochondrial membrane disruption, disappearance of the mitochondrial cristae, and size shrinkage.

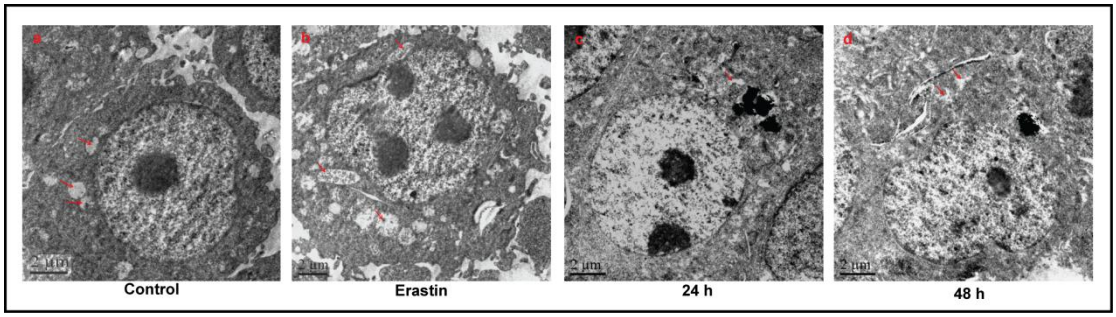

Figure 7. Morphology of mitochondria (red arrow) in nanoparticle (NP)-treated macrophages. (a–d): Untreated Ana-1 as control group (a), Ana-1 treated with erastin (25 μM) for 24 h (b); Transmission electron micrographs of NP treated cells for 24 h (c), 48 h (d). Ob: 2500×.

Discussion

As Fe_3O_4 NPs show high biodegradability, low biotoxicity, are easy to synthesize, and are magnetic by nature [43]; owing to these features, they are widely used in biotechnology and medicine. NPs were originally developed for improving the contrast of MRI [44, 45], that has been partially used in clinical applications [46]. Fe_3O_4 NPs are widely used in the magnetic hyperthermia treatment of tumors because of their high thermal effect in an oscillating magnetic field [47]. Because of their magnetic properties, NPs are easy to modify, and are therefore commonly used as drugs and gene to targeted delivery [48]. Notably, Fe_3O_4 NPs are also the first NPs that were found to have enzymatic activity [49]. These NPs possess antitumor effects that are mediated via the Fenton reaction [50], indicating their diverse applications in cancer treatment. Focusing on their ability to alter macrophage phenotypes, Zanganeh et al. [8] revealed that ferumoxytol inhibits cancer growth by inducing a pro-inflammatory immune response through M1 polarization. This study provides more evidence to

the antitumor activity of Fe_3O_4 NPs. NPs are usually administered via the intravenous route for clinical applications [51]. Biodistribution studies have demonstrated that the uptake of NPs by reticuloendothelial system (RES)macrophages may be the ultimate fate for most NPs, followed by being dissolved and metabolized in the autolysosomes [51, 52]. Although NPs are so widely used in the field of biotechnology, their cytotoxicity has not been fully explored.

TAMs can be functionally categorized into mixed type M1 and M2 macrophages, of which M2 accounts for a large proportion [53]. M1 and M2 macrophages are characterized by a high expression of nitric oxide (NO) producing iNOS and ornithine producing Arg-1, respectively, which correlate to either cytotoxic or repairing functions. TAMs are also known to express high levels of the anti-inflammatory cytokine IL-10. In this study, we found that the macrophage phenotypes changed following 48 h of exposure to NPs (Fig. 3), demonstrating that NPs not only polarized the macrophages into the M1 type, and also repolarized TAMs into M1 type, corroborating a previous report [8]. This implies that Fe_3O_4 NPs can be used for cancer treatment by means of immunotherapy. Notably, as the exposure time increased from 24 h to 48 h, the viability of the macrophages decreased with phenotype change (Fig. 2).

In order to evaluate the level of NP uptake, we measured the time gradient change of the intracellualr NPs (Fig. 4a). Consequently, we found that the cell uptake of NPs was maximum at 8 h, following which there was no significant increase in the NP content, suggesting that the reduction was partly mediated by exocytosis. Therefore, it was considered that the decrease in cell viability at 48 h was not related to the intracellular NP levels. We also found that intracellular NPs and lysosomes were colocalized and consider that the phagocytic capacity of macrophages and the concentration gradient between the outer and inner membranes are the underlying reasons for the colocalization. Supposedly,

NPs entered the Ana-1 cells, where some of them were taken up by lysosomes while some were degraded into iron ions[54].

Excessive iron ions in cells can cause abnormal iron metabolism and oxidative stress, accompanying ROS production [32]. We found that the production of intracellular ROS increased proportionally to the exposure time of NPs, suggesting that the presence of NPs correlates with ROS production in the cells. ROS has always been known as an important mediator of inducing cell death in several biological and pathological conditions[55]. Mitochondrial damage often occurrs owing to ROS production and subsequently causes cell death, where decrease in MMP level is considered a hallmark in apoptosis or ferroptosis. In this study, we found no prominent change in MMP in the 24 h group, suggesting that accumulated ROS increased mitochondrial damage and further induced apoptosis or ferroptosis.

Ferroptosis is a newly described programmed cell death pathway that is iron-dependent and different from apoptosis, necrosis, and autophagy. Its most important characteristic is the production of ROS, which is mainly caused by dysregulated iron metabolism. To explore the effects of NPs on the macrophages, we sequenced the mRNA of the cells exposured to NPs for 24 h and 48 h. According to the RNA-seq results illustrated in Fig. 6a, NPs activated the ferroptosis pathway by inducing *p53* expression after exposure for 48 h. The tumor suppressor gene, *p53*, plays an important role in the induction of ferroptosis by inhibiting the transcription of *SLC7A11*, which encodes the substrate-specific subunit of system Xc^- [56, 57], which is only found in cancer cells [58]. Jiang et al. [59] showed that p53 inhibits cystine uptake by transcriptionally suppressing *SLC7A11* thereby leading to increased sensitivity of ROS-induced ferroptosis in p53-activated cells.

Erastin, also known as ferroptosis-inducer, can enhance the sensitivity of cancer cells to chemotherapy and radiation, suggesting that it can be used as a new anticancer drug [35]. Since erastin can mediate perroptosis through p53 and other molecules, we used it as a positive control for ferroptosis in this study. We found that TFR level, which is a marker of ferroptosis, was higher in the erastin- and NP-treated groups than that in control group, indicating that NP-induced ferroptosis led to decreased cell activity. The expression levels of p53 and xCT were similar to that of the erastin group, corroborating p53-mediated ferroptosis of macrophages. Currently, targeting TAMs by either eliminating them or inducing their repolarization into the M1 (tumor suppressive type) phenotype is currently a hot topic in antitumor immunotherapy research.

Conclusion

In this study, we found that NPs could induce phenotypic changes and ferroptosis in macrophages. By analyzing the intracellular ROS levels and changes in MMP and mitochondrial morphology, we indicated that the ferroptosis-like cell death of macrophage increased as the exposure time increased. Furthermore, we showed that NPs induced macrophage ferroptosis mediated by p53 using RNA-seq and western blotting. These results provide a basis for further investigations into the precise molecular mechanism and related signaling pathways involved in ferroptosis induced by Fe_3O_4 NPs in macrophages and allows for the determination of the cytotoxicity of Fe_3O_4 NPs in vivo. Importantly, this work can provide a basis for the application of Fe_3O_4 NPs in the medical field for the inhibition of tumor cell growth via the induction of ferroptosis in macrophages.

Methods

NP synthesis and characterization

Fe_3O_4 NPs (100 nm diameter) were fabricated by a hydrothermal method using $FeCl_3$ and $NaAc·3H_2O$. Briefly, $FeCl_3$ was added to the solvent containing diethylene glycol and dissolved by ultrasonication. Then, $NaAc·3H_2O$ was added to this mixture and completely dissolved. The solution was autoclaved at 200°C for 12 h. Then the reactants were dried at 65°C after washed. The morphology and diameter of the NPs were determined using a transmission electron microscope (TEM Tecnai G2F30 S-TWIN; Hillsboro, NC, USA) and a scanning electron microscope (SEM S-4800; Hitachi, Tokyo, Japan). The particle size and zeta potentials of the NPs were measured using dynamic light scattering (Nano ZS90; Malvern, Inc., Malvern, UK).

Cell culturing

The mouse macrophage cell lines Ana-1 and lung cancer cell lines LLC (Lewis lung cancer cells) were obtained from the Cell Bank of the Chinese Academy of Sciences (Shanghai, China). Both cells were grown in RPMI 1640 (Gibco, New York, USA) culture medium supplemented with 10% FBS (Gibco) in a humidified atmosphere of 5% CO_2 at 37°C.

Cell viability analysis

Cultured Ana-1 cells were centrifuged at 400 ×g for 5min, and counted. One hundred microliters of cell suspension (1×10^5 cells/mL) was prepared, added to a 96-well plate. NPs at concentrations of 200, 300, 400 and 500 μg/mL were added to the cultures. After 24 and 48 h of co-incubation, 10 μL of CCK-8 solution and 100 μL of culture solution were added to each well and incubated at 37°C for 1 h. The absorbance of the solution was measured using a microplate reader (Epoch, Biotek, Winooski, VT, USA) at 450 nm.

Analysis of the effect of Fe_3O_4 NPs on macrophage phenotypes

To determine the effect of NPs on macrophages phenotypes. Ana-1 cells (1×10^6 cells/well) were seeded in 6-well plates and incubated for 12 h. Cells were collected for further analyses after exposed to 400 μg/mL NPs for 24 h and 48 h.

Construction of TAM model

The methods described by Wu et al. [60, 61] were used to construct the TAM model. When LLC cells reached 70% confluence, the conditioned medium (CM) was stored at -80°C after harvested and centrifuged at 1000 × *g* for 5 min. Next, after 12 h incubation of Ana-1 cells (1×10^6 cells/well) in 6-well plates, the culture medium was replaced with CM (2 mL/well), followed by incubation for 48 h, after which Ana-1 cells became TAMs. Finally, TAMs were incubated with 400 μg/mL NPs in 2 mL of fresh culture medium. After exposure for another 24 h and 48 h, the cells were harvested for further analyses.

Uptake of Fe_3O_4 NPs

NP uptake was analyzed by measuring intracellular iron by inductively coupled plasma-atomic emission spectrometry (ICP-ACE Optima 7300 DV; PerkinElmer, Waltham, MA, USA). Briefly, Ana-1 cells and NP solution were co-cultured for 2, 4, 8, 12, and 24 h. After washing with PBS three times to remove free NPs, the cells were collected and counted in each sample, followed by cell pelleting by centrifugate at 400g ×g for 5min. Dry the pellets and dissolved them in 100 μL of 65% nitric acid for 2 h at 70°C. Then, 900 μL of distilled water was added, and the emission spectra of samples were analyzed.

Intracellular localization of Fe_3O_4 NPs

Ana-1 cells were seeded in 12-well plates with slides and incubated with a fresh cell culture medium containing NPs (400 μg/mL) for up to 8 h. following incubation, cellular NPs were visualized and localized using Prussian blue staining (Solarbio, Beijing, China) and Lyso-Tracker Red fluorescent probes (Beyotime, Shanghai, China) according to the manufacturers' instructions.

For Prussian blue staining, the cells were washed with PBS two times to remove the free NPs. The slides with NP-loaded Ana-1 cells were immersed in ddH_20 for 5 min before incubation in Prussian blue dying solution for 20 min. The slides were washed and counterstained with neutral red for 2 min before washing and mounting in an aqueous fixative. Images of slides were obtained using a light microscope (CX23; Olympus, Tokyo, Japan). The Lyso-Tracker Red staining for NPs intracellular localization, slides were incubated with 1 mL of Hank's balanced salt solution (HBSS, Beyotime) containing 50 nM Lyso-Tracker Red, which efficiently diffuses into living cells to visually detect lysosomes. Images were obtained using a fluorescence microscope (ELOS FL Auto; Thermo Fisher, Waltham, MA, USA).

Detection of ROS

Intracellular ROS was detected using the fluorescent probe DCFH-DA in the ROS Detection kit (Beyotime). The cells were collected by centrifugated at 400g × for 5min, resuspended in diluted DCFH-DA, and incubated at 37°C for 20 min. Cells were resuspended in PBS after centrifugated, the fluorescence intensity of the cells was analyzed using a flow cytometer (FCM LSRFormanc; BD, Franklin Lakes, NJ, USA). Rosup is a compound mixture with a concentration of 50mg/ mL which treated the cells for 20 min as a positive control reagent to facilitate the detection of ROS.

Analysis of mitochondrial damage

MMP was measured using an MMP Assay Kit (Solarbio) of tetraethylbenzimidazolyl carbocyanineiodide (JC-1). The cell suspension (1 × 10^6 cells/mL, 0.5 mL) supplemented. The cells were incubated with 0.5 mL of JC-1 at 37°C for 20 min. Based on the color change, MMP was detected using a fluorescence microscope, and the ratio of red/green fluorescence intensity was evaluated using a microplate reader (SYNERGY2, Bio-Tek, Winooski, VT, USA) to determine the degree of mitochondrial damage. Untreated cells were exposed to 10 μM carbonyl cyano-p-chlorophenylhydrazone (CCCP) for 20 min as a positive control; CCCP causes the complete loss of MMP.

RNA-sequencing

After cells were harvested, intracellular RNA was extracted using the TRIzol reagent (Takara, Tokyo, Japan), and RNA samples were analyzed by high-throughput transcriptome sequencing technology in Science and technology company (E-gene, Shenzhen, China).

Ultramicroscopic analysis of cells

The microstructure of the NP-treated Ana-1 cells were observed by a TEM. Briefly, Ana-1 cells were treated with NPs (400 μg/mL) for 24 h and 48 h or Erastin (25 μM; MCE, Princeton, NJ, USA) for 24 h. Cells were fixed in 4% glutaraldehyde for an additional 12-24 h followed by 4°C. Next, the cells were post-fixed with 1% OsO_4 and embedded in Epon. Ultrathin sections were visualized using a Hitachi-7500 TEM (Hitachi, Tokyo, Japan). Erastin, an inducer of ferroptosis, was used as a positive control for induce of ferroptosis.

Western blotting

After cell lysis and protein extraction by total protein extraction kit (KeyGEN, Jiangsu, China). The PVDF membrane with proteins was incubated with primary rabbit antibody specific for iNOS, Arg-1 (CST, Massachusetts, USA), TFR, p53, xCT (Abcam, Massachusetts, USA)and respective secondary antibody (1:4000). This was followed by visualization using an ECL system. Protein expression levels were standardized using tubulin or β-actin.

Reverse transcription–quantitative PCR (RT–qPCR)

The purified RNA was reverse transcribed using the Transcriptor cDNA Synthesis Kit (TaKara, Tokyo, Japan). The resultant cDNA was subjected to qPCR using the Light Cycler 96 (Roche, Basel, Switzerland). *GAPDH* used as a reference gene to analyze the *iNOS, Arg-1, IL-10* gene quantitatively. Relative gene expression was quantified using the $2^{-\Delta\Delta Ct}$ method.

Statistical analysis

Data are expressed as means ± standard error of mean (SEM) and all statistical analyses were performed using GraphPad Prism 8 (La Jolla, CA, USA). All reactions were performed in triplicate, and each experiment was repeated three times. Results were analyzed by a two-way anova.

Declarations

Ethics approval and consent to participate: Not applicable

Consent for publication: Not applicable

Availability of data and materials: We ensure the authenticity and repeatability of the data obtained by this research. All data generated or analyzed during this study are included in this published article.

Competing interests: The authors declare that they have no competing interests.

Funding: This work was supported by the National Natural Science Foundation of China (Grant No.81770018) and the Postgraduate Scientific Research and Innovation Projects of YangZhou University (XKYCX19-153).

Authors' contributions:

WC contributed to the idea of the study, participated in the research planning and experiment design. SZM, ZBY, SF, LY, LY carried out the concepts, design, the definition of intellectual content, literature search, data acquisition, data analysis, and manuscript preparation. WC performed the data analyses and wrote the manuscript. SHC finally checked all the data and the manuscript. All authors read and approved the final manuscript.

References

1. Shen L, Li B, Qiao Y. Fe3O4 Nanoparticles in Targeted Drug/Gene Delivery Systems. Materials. 2018;11(2):324. 10.3390/ma11020324.
2. He K, Ma Y, Yang B, Liang C, Chen X, Cai C. The efficacy assessments of alkylating drugs induced by nano-Fe3O4/CA for curing breast and hepatic cancer. Spectrochimica Acta Part A: Molecular and Biomolecular Spectroscopy. 2017;173:82-86. 10.1016/j.saa.2016.08.047.
3. Shahabadi N, Akbari A, Jamshidbeigi M, Falsafi M. Functionalization of Fe3O4@SiO2 magnetic nanoparticles with nicotinamide and in vitro DNA interaction. J Mol Liq. 2016;224:227-233. 10.1016/j.molliq.2016.09.103.
4. Ma M, Yan F, Yao M, Wei Z, Zhou D, Yao H, et al. Template-Free Synthesis of Hollow/Porous Organosilica-Fe3O4 Hybrid Nanocapsules toward Magnetic Resonance Imaging-Guided High-Intensity Focused Ultrasound Therapy. ACS Appl Mater Interfaces. 2016;8(44):29986-29996. 10.1021/acsami.6b10370.
5. Seeni RZ, Yu X, Chang H, Chen P, Liu L, Xu C. Iron Oxide Nanoparticle-Powered Micro-Optical

Coherence Tomography for in Situ Imaging the Penetration and Swelling of Polymeric Microneedles in the Skin. Acs Appl Mater Inter. 2017;9(24):20340-20347. 10.1021/acsami.7b00481.

6. Nan X, Zhang X, Liu Y, Zhou M, Chen X, Zhang X. Dual-Targeted Multifunctional Nanoparticles for Magnetic Resonance Imaging Guided Cancer Diagnosis and Therapy. Acs Appl Mater Inter. 2017;9(11):9986-9995. 10.1021/acsami.6b16486.

7. Luong D, Sau S, Kesharwani P, Iyer AK. Polyvalent Folate-Dendrimer-Coated Iron Oxide Theranostic Nanoparticles for Simultaneous Magnetic Resonance Imaging and Precise Cancer Cell Targeting. Biomacromolecules. 2017;18(4):1197-1209. 10.1021/acs.biomac.6b01885.

8. Zanganeh S, Hutter G, Spitler R, Lenkov O, Mahmoudi M, Shaw A, et al. Iron oxide nanoparticles inhibit tumour growth by inducing pro-inflammatory macrophage polarization in tumour tissues. Nat Nanotechnol. 2016;11(11):986-994. 10.1038/nnano.2016.168.

9. Denardo DG, Ruffell B. Macrophages as regulators of tumour immunity and immunotherapy. Nature reviews. Immunology. 2019;19(6):369-382. 10.1038/s41577-019-0127-6.

10. Mills CD, Lenz LL, Harris RA. A Breakthrough: Macrophage-Directed Cancer Immunotherapy. Cancer Res. 2016;76(3):513-516. 10.1158/0008-5472.CAN-15-1737.

11. Muntimadugu E, Kommineni N, Khan W. Exploring the Potential of Nanotherapeutics in Targeting Tumor Microenvironment for Cancer Therapy. Pharmacol Res. 2017;126:109-122. 10.1016/j.phrs.2017.05.010.

12. Alphandéry E. Biodistribution and targeting properties of iron oxide nanoparticles for treatments of cancer and iron anemia disease. Nanotoxicology. 2019;13(5):573-596. 10.1080/17435390.2019.1572809.

13. Dixon SJ, Lemberg KM, Lamprecht MR, Skouta R, Zaitsev EM, Gleason CE, et al. Ferroptosis: An Iron-Dependent Form of Nonapoptotic Cell Death. Cell. 2012;149(5):1060-1072. 10.1016/j.cell.2012.03.042.

14. Friedmann Angeli JP, Schneider M, Proneth B, Tyurina YY, Tyurin VA, Hammond VJ, et al. Inactivation of the ferroptosis regulator Gpx4 triggers acute renal failure in mice. Nat Cell Biol. 2014;16(12):1180-1191. 10.1038/ncb3064.

15. Jiang M, Qiao M, Zhao C, Deng J, Li X, Zhou C. Targeting ferroptosis for cancer therapy: exploring novel strategies from its mechanisms and role in cancers. Translational Lung Cancer Research. 2020;9(4):1569-1584. 10.21037/tlcr-20-341.

16. Tang D, Kang R, Berghe TV, Vandenabeele P, Kroemer G. The molecular machinery of regulated cell death. Cell Res. 2019;29(5):347-364. 10.1038/s41422-019-0164-5.

17. Liang H, Guo J, Shi Y, Zhao G, Sun S, Sun X. Porous yolk-shell Fe/Fe3O4 nanoparticles with controlled exposure of highly active Fe(0) for cancer therapy. Biomaterials. 2021;268:120530.

10.1016/j.biomaterials.2020.120530.

18. Zhang Y, Xia M, Zhou Z, Hu X, Wang J, Zhang M, et al. p53 Promoted Ferroptosis in Ovarian Cancer Cells Treated with Human Serum Incubated-Superparamagnetic Iron Oxides. 2021;Volume 16:283-296. 10.2147/IJN.S282489.

19. Zheng H, You J, Yao X, Lu Q, Guo W, Shen Y. Superparamagnetic iron oxide nanoparticles promote ferroptosis of ischemic cardiomyocytes. J Cell Mol Med. 2020;24(18):11030-11033. 10.1111/jcmm.15722.

20. Seibt TM, Proneth B, Conrad M. Role of GPX4 in ferroptosis and its pharmacological implication. Free radical biology & medicine. 2019;133:144-152. 10.1016/j.freeradbiomed.2018.09.014.

21. Dixon SJ, Patel DN, Welsch M, Skouta R, Lee ED, Hayano M, et al. Pharmacological inhibition of cystine–glutamate exchange induces endoplasmic reticulum stress and ferroptosis. Elife. 2014;3. 10.7554/eLife.02523.

22. Jiang L, Kon N, Li T, Wang S, Su T, Hibshoosh H, et al. Ferroptosis as a p53-mediated activity during tumour suppression. Nature. 2015;520(7545):57-62. 10.1038/nature14344.

23. Kang R, Kroemer G, Tang D. The tumor suppressor protein p53 and the ferroptosis network. Free Radical Bio Med. 2019;133:162-168. 10.1016/j.freeradbiomed.2018.05.074.

24. Saint-Germain E, Mignacca L, Vernier M, Bobbala D, Ilangumaran S, Ferbeyre G. SOCS1 regulates senescence and ferroptosis by modulating the expression of p53 target genes. Aging (Albany, NY.). 2017;9(10):2137-2162. 10.18632/aging.101306.

25. Wang S, Li D, Ou Y, Jiang L, Chen Y, Zhao Y, et al. Acetylation Is Crucial for p53-Mediated Ferroptosis and Tumor Suppression. Cell Rep. 2016;17(2):366-373. 10.1016/j.celrep.2016.09.022.

26. Zhang S, Shu W, Yiru S, Yunqi X, Shi LGAS. Cytotoxicity studies of Fe3O4 nanoparticles in chicken macrophage cells. R Soc Open Sci. 2020;(74(4)).

27. Parayath NN, Parikh A, Amiji MM. Repolarization of Tumor-Associated Macrophages in a Genetically Engineered Nonsmall Cell Lung Cancer Model by Intraperitoneal Administration of Hyaluronic Acid-Based Nanoparticles Encapsulating MicroRNA-125b. Nano Lett. 2018;18(6):3571-3579. 10.1021/acs.nanolett.8b00689.

28. Blasi E, Pitzurra L, Bartoli A, Puliti M, Bistoni F. Tumor necrosis factor as an autocrine and paracrine signal controlling the macrophage secretory response to Candida albicans. Infect Immun. 1994;62(4):1199-206. 10.1128/IAI.62.4.1199-1206.1994.

29. Cox GW, Mathieson BJ, Gandino L, Blasi E, Radzioch D, Varesio L. Heterogeneity of hematopoietic cells immortalized by v-myc/v-raf recombinant retrovirus infection of bone marrow or fetal liver. JNCI : Journal of the National Cancer Institute. 1989;81(19):1492-1496. 10.1093/jnci/81.19.1492.

30. Cairo G, Recalcati S, Mantovani A, Locati M. Iron trafficking and metabolism in macrophages:

contribution to the polarized phenotype. Trends Immunol. 2011;32(6):241-247. 10.1016/j.it.2011.03.007.

31. Wu T, Li Y, Wu T, Chang JWC, Chou W, Hsieh L, et al. Culture supernatants of different colon cancer cell lines induce specific phenotype switching and functional alteration of THP-1 cells. Cell Immunol. 2014;290(1):107-115. 10.1016/j.cellimm.2014.05.015.

32. Zhang Y, Hai Y, Miao Y, Qi X, Xue W, Luo Y, et al. The toxicity mechanism of different sized iron nanoparticles on human breast cancer (MCF7) cells. Food Chem. 2021;341:128263. 10.1016/j.foodchem.2020.128263.

33. Vanden Berghe T, Linkermann A, Jouan-Lanhouet S, Walczak H, Vandenabeele P. Regulated necrosis: the expanding network of non-apoptotic cell death pathways. Nature reviews. Molecular cell biology. 2014;15(2):135-147. 10.1038/nrm3737.

34. Feng H, Schorpp K, Jin J, Yozwiak CE, Hoffstrom BG, Decker AM, et al. Transferrin Receptor Is a Specific Ferroptosis Marker. Cell Rep. 2020;30(10):3411-3423.e7. 10.1016/j.celrep.2020.02.049.

35. Li Y, Wang X, Yan J, Liu Y, Yang R, Pan D, et al. Nanoparticle ferritin-bound erastin and rapamycin: a nanodrug combining autophagy and ferroptosis for anticancer therapy. Biomater Sci. 2019;7(9):3779-3787. 10.1039/c9bm00653b.

36. Gnanapradeepan K, Basu S, Barnoud T, Budina-Kolomets A, Kung C, Murphy ME. The p53 Tumor Suppressor in the Control of Metabolism and Ferroptosis. Front Endocrinol. 2018;9. 10.3389/fendo.2018.00124.

37. Huang C, Yang M, Deng J, Li P, Su W, Jiang R. Upregulation and activation of p53 by erastininduced reactive oxygen species contribute to cytotoxic and cytostatic effects in A549 lung cancer cells. Oncol Rep. 2018;40(4):2363-2370. 10.3892/or.2018.6585.

38. Shintoku R, Takigawa Y, Yamada K, Kubota C, Yoshimoto Y, Takeuchi T, et al. Lipoxygenase-mediated generation of lipid peroxides enhances ferroptosis induced by erastin and RSL3. Cancer Sci. 2017;108(11):2187-2194. 10.1111/cas.13380.

39. Zhou B, Liu J, Kang R, Klionsky DJ, Kroemer G, Tang D. Ferroptosis is a type of autophagy-dependent cell death. Semin Cancer Biol. 2020;66:89-100. 10.1016/j.semcancer.2019.03.002.

40. Yu H, Guo P, Xie X, Wang Y, Chen G. Ferroptosis, a new form of cell death, and its relationships with tumourous diseases. J Cell Mol Med. 2017;21(4):648-657. 10.1111/jcmm.13008.

41. Dehart DN, Fang D, Heslop K, Li L, Lemasters JJ, Maldonado EN. Opening of voltage dependent anion channels promotes reactive oxygen species generation, mitochondrial dysfunction and cell death in cancer cells. Biochem Pharmacol. 2018;148:155-162. 10.1016/j.bcp.2017.12.022.

42. Battaglia AM, Chirillo R, Aversa I, Sacco A, Costanzo F, Biamonte F. Ferroptosis and Cancer:

Mitochondria Meet the “Iron Maiden” Cell Death. Cells-Basel. 2020;9(6):1505. 10.3390/cells9061505.

43. Zhao Z, Zhou Z, Bao J, Wang Z, Hu J, Chi X, et al. Octapod iron oxide nanoparticles as high-performance T2 contrast agents for magnetic resonance imaging. Nat Commun. 2013;4(1). 10.1038/ncomms3266.

44. Yuan Y, Ding Z, Qian J, Zhang J, Xu J, Dong X, et al. Casp3/7-Instructed Intracellular Aggregation of Fe3 O4 Nanoparticles Enhances T2 MR Imaging of Tumor Apoptosis. Nano Lett. 2016;16(4):2686-2691. 10.1021/acs.nanolett.6b00331.

45. Li J, Wang S, Shi X, Shen M. Aqueous-phase synthesis of iron oxide nanoparticles and composites for cancer diagnosis and therapy. Adv Colloid Interfac. 2017;249:374-385. 10.1016/j.cis.2017.02.009.

46. Malhotra N, Lee J, Liman RAD, Ruallo JMS, Villaflores OB, Ger T, et al. Potential Toxicity of Iron Oxide Magnetic Nanoparticles: A Review. Molecules. 2020;25(14):3159. 10.3390/molecules25143159.

47. Sharma SK, Shrivastava N, Rossi F, Tung LD, Thanh NTK. Nanoparticles-based magnetic and photo induced hyperthermia for cancer treatment.; 2019. pp. 100795.

48. Zhao S, Yu X, Qian Y, Chen W, Shen J. Multifunctional magnetic iron oxide nanoparticles: an advanced platform for cancer theranostics. Theranostics. 2020;10(14):6278-6309. 10.7150/thno.42564.

49. Zhang J, Wang T, Gao L, Perrett S, Feng J, Zhang Y, et al. Intrinsic peroxidase-like activity of ferromagnetic nanoparticles. Nat Nanotechnol. 2007;2(9):577-583. 10.1038/nnano.2007.260.

50. Gobbo OL, Sjaastad K, Radomski MW, Volkov Y, Prina-Mello A. Magnetic Nanoparticles in Cancer Theranostics. Theranostics. 2015;5(11):1249-1263. 10.7150/thno.11544.

51. Jin R, Liu L, Zhu W, Li D, Yang L, Duan J, et al. Iron oxide nanoparticles promote macrophage autophagy and inflammatory response through activation of toll-like Receptor-4 signaling. Biomaterials. 2019;203:23-30. 10.1016/j.biomaterials.2019.02.026.

52. Xia W, Song H, Wei Q, Wei A. Differential response of macrophages to core‐shell Fe3O4@Au nanoparticles and nanostars. Nanoscale. 2012;4(22):7143. 10.1039/c2nr32070c.

53. Denardo DG, Ruffell B. Macrophages as regulators of tumour immunity and immunotherapy. Nat Rev Immunol. 2019;19(6):369-382. 10.1038/s41577-019-0127-6.

54. Auerbach M, Macdougall I. The available intravenous iron formulations: History, efficacy, and toxicology. Hemodial Int. 2017;21:S83-S92. 10.1111/hdi.12560.

55. Dixon SJ, Stockwell BR. The role of iron and reactive oxygen species in cell death. Nat Chem Biol. 2014;10(1):9-17. 10.1038/nchembio.1416.

56. Tarangelo A, Magtanong L, Bieging-Rolett KT, Li Y, Ye J, Attardi LD, et al. p53 Suppresses Metabolic Stress-Induced Ferroptosis in Cancer Cells. Cell Rep. 2018;22(3):569-575. 10.1016/j.celrep.2017.12.077.

57. Dixon SJ, Stockwell BR. The Hallmarks of Ferroptosis. Annual review of cancer biology. 2019;3(1):35-54. 10.1146/annurev-cancerbio-030518-055844.

58. Li Y, Cao Y, Xiao J, Shang J, Tan Q, Ping F, et al. Inhibitor of apoptosis-stimulating protein of p53 inhibits ferroptosis and alleviates intestinal ischemia/reperfusion-induced acute lung injury. Cell Death & Differentiation. 2020;27(9):2635-2650. 10.1038/s41418-020-0528-x.

59. Jiang L, Kon N, Li T, Wang S, Su T, Hibshoosh H, et al. Ferroptosis as a p53-mediated activity during tumour suppression. Nature. 2015;520(7545):57-62. 10.1038/nature14344.

60. Zhu Y, Chen X, Pan Q, Wang Y, Su S, Jiang C, et al. A Comprehensive Proteomics Analysis Reveals a Secretory Path- and Status-Dependent Signature of Exosomes Released from Tumor-Associated Macrophages. J Proteome Res. 2015;14(10):4319-4331. 10.1021/acs.jproteome.5b00770.

61. Colegio OR, Chu N, Szabo AL, Chu T, Rhebergen AM, Jairam V, et al. Functional polarization of tumour-associated macrophages by tumour-derived lactic acid. Nature. 2014;513(7519):559-563. 10.1038/nature13490.